nature communications

Article | Article in Press

https://doi.org/10.1038/s41467-026-78726-z

Ikaros transcription factors prevent the activation of an endothelial cell program in bone marrow hematopoietic stem and progenitor cells

Received: 26 January 2026

Accepted: 30 September 2026

Published online: 18 November 2026

Check for updates

Chiara Taroni[1,2,3,4,9], Geoffrey Bianchi[1,2,3,4,9], Mahassen El Khoury[1,2,3,4], Mari Carmen Romero-Mulero[5,6,7], Nina Cabezas-Wallscheid[5,7], Susan Chan[1,2,3,4] ✉, Philippe Kastner[1,2,3,4,8] ✉ & Peggy Kirstetter[1,2,3,4] ✉

Hematopoietic stem cells (HSCs) are generally committed to the hematopoietic lineage, but how that commitment is maintained is not well understood. We show that the Ikaros family of transcription factors is essential for HSC identity. Ikaros, alone or in combination with Helios, is required to sustain the pool of multipotent HSCs and their downstream progenitor cells in adult animals, by directly repressing a core group of genes implicated in wound healing, cell junction organization, and actin cytoskeleton organization. Remarkably, upon in vivo or in vitro deletion of Ikaros or Ikaros+Helios, nearly one-third of the hematopoietic stem and progenitor cells (HSPCs) rapidly exhibit an endothelial cell transcriptomic signature, and develop non-hematopoietic structures resembling CD144+ endothelial-like cells. These results indicate that adult HSPCs are highly plastic and prevented from activating an endothelial cell program by Ikaros family transcription factors.

Hematopoietic stem cells (HSCs) and their downstream multipotent progenitors (MPPs) form the hematopoietic stem and progenitor cell (HSPC) pool in the adult bone marrow (BM), which is responsible for the continuous production of erythroid, myeloid, and lymphoid cells. HSPCs have historically been considered to be multipotent but committed to the hematopoietic lineage[1–3]. Still, recent studies have questioned whether these cells are irreversibly committed and suggested that at least a small percentage may retain cellular plasticity[4–7]. The molecular regulators that maintain HSC identity and prevent cell lineage reprogramming are not well understood.

The Ikaros transcription factor (TF) family is essential for hematopoiesis[8,9]. This family of homologous proteins is characterized by two conserved zinc finger domains that mediate DNA-binding at GGAA motifs and protein-protein dimerization[10–13]. These TFs bind DNA as homodimers or heterodimers, and activate or repress target gene expression for reasons still incompletely understood[14–17]. Ikaros (encoded by the *Ikzf1* gene) and Helios (*Ikzf2*) have been demonstrated to influence HSPC biology. Mice carrying germline-deleted null or dominant-negative *Ikzf1* mutations exhibit striking losses in BM HSPC frequency and reconstitution capacity, implicating Ikaros in HSC production or activity[18]. More recently, we reported that animals bearing germline- or conditionally-deleted *Ikzf2* had globally normal HSPC frequencies but increased megakaryocyte-biased progenitors, indicating that Helios helps to maintain HSC multipotency by repressing

[1]Département de Génomique Fonctionnelle et Cancer, Institut de Génétique et de Biologie Moléculaire et Cellulaire (IGBMC), ILLKIRCH, France. [2]Institut National de la Santé et de la Recherche Médicale (INSERM), U1258 ILLKIRCH, France. [3]Centre National de la Recherche Scientifique (CNRS), UMR7104 ILLKIRCH, France. [4]Université de Strasbourg, ILLKIRCH, France. [5]Max Planck Institute of Immunobiology and Epigenetics, Freiburg, Germany. [6]University of Freiburg, Faculty of Biology, Freiburg, Germany. [7]Laboratory of Stem Cell Biology and Ageing, Department of Health Sciences and Technology, Swiss Federal Institute of Technology (ETH Zürich), Zürich, Switzerland. [8]Faculté de Médecine, Université de Strasbourg, Strasbourg, France. [9]These authors contributed equally: Chiara Taroni, Geoffrey Bianchi. ✉e-mail: scpk@igbmc.fr; scpk@igbmc.fr; kirstett@igbmc.f

megakaryocyte priming[19]. These important but infrequent studies implicated both Ikaros and Helios in HSPC function, but major questions remained. For example, it was unknown why HSC activity is severely curtailed in Ikaros-deficient mice and which Ikaros- and Helios-targeted genes promote HSPC function in these mutant animals.

Here, we revisited the roles of Ikaros and Helios in HSC biology and showed that these factors are required to maintain hematopoietic identity by preventing the activation of an endothelial cell program in HSPCs.

Results

Ikaros and Helios are required for LT-HSC homeostasis

We first evaluated the relative protein abundance of both TFs in murine long- (LT-) and short-term (ST-) HSCs, MPP populations, and common lymphoid progenitors (CLP) by flow cytometry (Fig. 1a). Ikaros was increasingly expressed from HSCs to MPPs and CLPs. In contrast, Helios was similarly expressed across all HSPCs, with higher abundance in the erythro-megakaryocytic-biased MPP2 population, followed by much lower expression in CLPs, consistent with our previous results[19]. Thus, Ikaros and Helios are differentially expressed in HSPCs.

TF function was studied in conditional knockout (KO) animals carrying floxed *Ikzf1* and/or *Ikzf2* alleles together with a Rosa26-CreERT2 transgene. We evaluated the following genotypes: WT Cre- (*Ikzf1*$^{f/f}$ *Ikzf2*$^{f/f}$ Cre-); WT Cre+ (*Ikzf1*$^{+/+}$ *Ikzf2*$^{+/+}$ Cre +); Ikaros KO (*Ikzf1*$^{f/f}$ *Ikzf2*$^{+/+}$ Cre +); Helios KO (*Ikzf1*$^{+/+}$ *Ikzf2*$^{f/f}$ Cre +); double (D)KO (*Ikzf1*$^{f/f}$ *Ikzf2*$^{f/f}$ Cre +). Unless otherwise indicated, the WT samples came from WT Cre+ mice. Cre activity was induced by daily tamoxifen (TAM) injections over five days (Fig. 1b), and TF loss in the HSPCs (LSK, Lin- Sca1+ cKit +) was confirmed 5 days after the last injection (5 d post-TAM; Fig. 1b, right).

At 5 d post-TAM, the bone marrow (BM) cellularities were unaffected in the WT animals, but already reduced in the Helios or Ikaros KO as well as in the DKOs (Fig. 1c). In addition, the Lin- cKit+ cells, that include the HSPCs, were phenotypically altered, and HSPC frequencies were increased in the Helios KO samples (Fig. 1d). Between the WT Cre- and Cre+ controls, the HSPC compartment was also different (Fig.1a), indicating that cells with no floxed alleles are still susceptible to the effects of Cre-mediated toxicity[20,21], though only small differences were observed in BM cellularity and in the absolute numbers of HSPCs and LT-HSCs. Strikingly, there was a drastic reduction in LT-HSC (CD150 + CD48- LSK) frequencies in the mutant HSPC compartments (Fig. 1e). LT-HSCs were similarly lost among the HSPCs of germline-deleted Ikaros null and Helios+Ikaros null fetal livers (Fig.1b), and in the BM competitive transplantation experiments described below (Fig. 1f and S1d), supporting a direct link between Ikaros factors and LT-HSC maintenance, rather than a transient by-product of the Cre-induced inflammation. Further investigation of the mutant LT-HSCs revealed more cells in S/G2/M (Fig.1c), suggesting that Ikaros and Helios repress cell cycle entry.

Two weeks after TAM treatment (14 d post-TAM), the Ikaros KO and DKO mice continued to show severe abnormalities while hematopoiesis was generally restored in the WT and Helios KO mice. BM cellularity remained low in the Ikaros KO (~ 3-fold), and even lower in the DKO (~ 10-fold) (Fig. 2a), which was associated with a loss of peripheral blood monocytes, neutrophils and lymphocytes (Fig. 2b). Ikaros KO HSPCs were increased in frequency but showed reduced cKit expression levels (Fig. 2c). LT-HSCs continued to be almost non-existent in the Ikaros KO and DKO BM (Fig. 2d), suggesting that Ikaros loss impacts their long-term function. Indeed, the absolute numbers of all downstream progenitor cells (common myeloid, megakaryocyte-erythroid, granulocyte-monocyte) were low to zero in the Ikaros KO and DKO BM (Fig. 2e). Ikaros KO and DKO mice were anemic (Fig. 3a) and moribund by 14 d post-TAM (not shown). Erythroid differentiation in the Ikaros KO was blocked at the CD71 + TER119+ stage (Fig. 3b), in line with published results[22]. Interestingly, the DKO BM was more affected and lacked all erythroid progenitors starting at the MPP2 stage (Fig. 3b and not shown), even though the Helios KO animals appeared normal. Similar results were obtained in the DKO livers of germline-deleted E14.5 fetuses (Fig. 3c), indicating that both TFs are required for fetal and adult erythropoiesis.

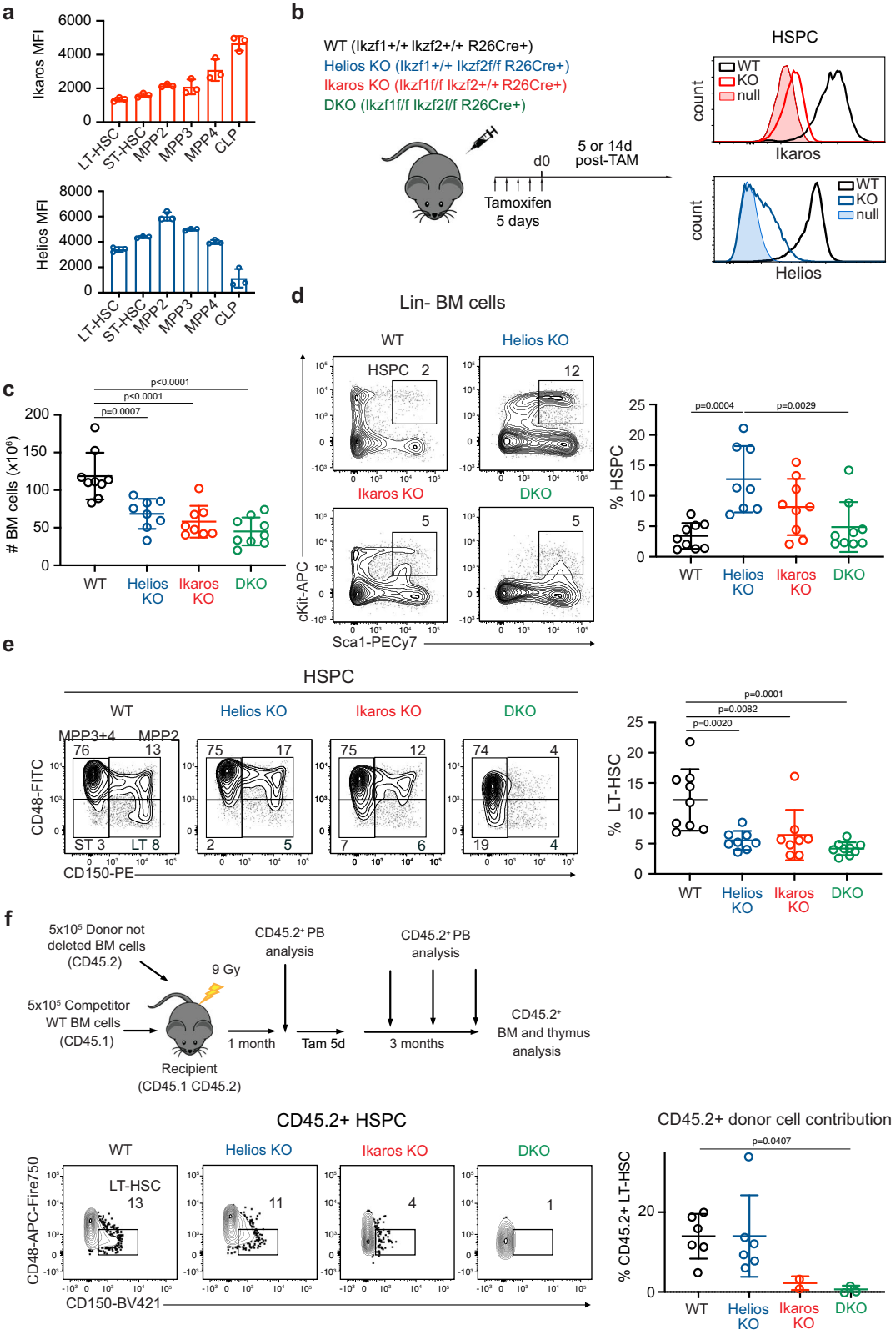
To assess LT-HSC functionality, we performed competitive transplantation experiments where the floxed alleles were deleted after repopulation (Fig. 1f, top). Equal numbers of CD45.2+ donor and CD45.1+ competitor WT BM cells were transferred into lethally-irradiated CD45.1 + CD45.2+ hosts, where the ratio of donor vs. competitor cells was similar (~1:1) across genotypes one month after transplantation (not shown). The recipient animals were then subjected to the 5 d TAM protocol, after which the peripheral blood was analyzed monthly, and the thymus and BM assessed after 3 months. Many (~75%) of the recipients transplanted with *Ikzf1*$^{f/f}$ ± *Ikzf2*$^{f/f}$ cells developed CD4 + CD8 + T cell lymphomas/leukemias in the thymus typically associated with Ikaros deficiency[23–25]; they were not studied further (not shown). Among the healthy animals (tumor-free in the thymus and BM), the contributions of Ikaros and Helios to BM LT-HSCs were evaluated, which revealed that the frequencies of CD45.2+ Ikaros KO and DKO LT-HSCs were drastically reduced compared with WT and Helios KO counterparts (Fig. 1f, bottom). Importantly, the frequencies of the competitor CD45.1 + LT-HSCs were similar across the board (Fig. 1d), indicating that extrinsic factors alone were not sufficient to induce the mutant LT-HSC phenotype. Thus, Ikaros and, to a smaller extent, Helios are intrinsically required for LT-HSC fitness.

Ikaros+Helios deficiency alters the HSPC composition and promotes dendritic cell (DC) differentiation

To assess the effects of Ikaros and Helios on HSPC gene expression, we performed a single cell (sc)RNA-sequencing analysis on cells from animals treated 5 d post-TAM. After quality control filtering, the HSPCs (2,283 WT; 4,638 Helios KO; 2,792 Ikaros KO; 2,761 DKO) were visualized with Uniform Manifold Approximation and Projection (UMAP) for dimension reduction, grouped into 6 clusters (Fig. 2a and S4a), and annotated according to published HSC and MPP signatures[26]. The HSC/MPP5 cluster was enriched for genes associated with stemness and early MPPs (MPP5 and, to a smaller extent, MPP1); the MPP5/4/3 cluster contained genes associated with the MPP5, previously identified as a master-type MPP that can give rise to most HSPC populations, including MPP1 (situated between HSCs and downstream MPP subsets) and the lymphoid-primed MPP4 and myeloid-primed MPP3 populations. These as well as the identified MPP2, MPP3 and MPP4 clusters were observed in both WT and mutant HSPCs (Fig. 2b). The HSC/MPP5 and MPP5/4/3 clusters were reduced in the single and double KO HSPCs, while the MPP2 cluster was slightly increased in the Helios KO but reduced in the Ikaros KO and DKO samples; accordingly, the MPP3 and −4 clusters were proportionally increased in the mutants (Fig. 4b).

Unexpectedly, we detected a “DC-like” cluster that, while marginally present in the WT and Helios KO HSPCs, was significantly increased in the Ikaros KO and DKO samples, and accounted for ~13% of the DKO cells (Fig. 2c). These cells co-expressed genes associated with MPP2-4, but especially MPP4, cells (though not the MPP4-defining *Dntt*) (Fig. 4c). We defined a gene expression signature for this cluster as the top 50 genes that were upregulated in Ikaros KO and DKO DC-like cells with respect to cognate mutant MPP4 cells (Table S1). The signature was then compared with expression profiles from a diverse set of hematopoietic cell types (Immgen database), which revealed that the DC-like signature was enriched among conventional DCs, particularly CD8+ DCs, macrophages and monocytes (Fig. 2d). Numerous genes involved in antigen presentation (*H2-EbA*, *H2-Aa*, *H2-Ab1*, *H2-DMb1*, *Cd74*, *Ifi30*, *Psap*, *Mpeg1*, *Wdfy4*) were upregulated in the DC-like cluster (Fig. 2d–f). This cluster also included *Batf3* (a key

https://doi.org/10.1038/s41467-026-78726-z



regulator of CD8+ DCs), *Cd8a*, and *Apol7c*, all markers commonly associated with DCs. Interestingly, some genes, like *Cd74*, were also upregulated in other mutant populations (Fig. 2e). Indeed, CD11c +MHCII+CD8a+ cells were prominent among the Ikaros KO and DKO HSPCs after 5 d post-TAM treatment (Fig. 2g). Thus, Ikaros, alone or together with Helios, represses a dendritic cell gene expression program in hematopoietic progenitor cells.

Ikaros regulates the expression of numerous HSPC genes

To study the gene expression changes associated with Ikaros and Helios binding, we studied the murine HPC7 multipotent progenitor cell line to first identify the targets of these TFs. This cell line expresses both Ikaros and Helios, and is composed of cells with HSPC and Lin-cKit+Sca1- features that differentiate into multiple hematopoietic lineages in the presence of appropriate cytokines[27]. Ikaros and Helios

Fig. 1 | Ikaros and Helios are required to maintain LT-HSCs. a Ikaros (top) and Helios (bottom) median fluorescence intensity (MFI) in the indicated populations, as measured by flow cytometry. Data from 3 independent experiments. **b** Left: strategy of Ikaros and/or Helios TAM-induced inactivation in vivo. Right: loss of Ikaros (red line) and Helios (blue line) protein by flow in the respective KO HSPCs 5 d post-TAM compared with Ikaros-null and Helios-null HSPCs (representative of all KO experiments performed). **c** BM cellularity (tibias, femurs, pelvis, sternum) of mice 5 d post-TAM. Mean ± SD are shown for all graphs. **d** Representative contour plots (left) of lineage negative (Lin-) cells stained for cKit and Sca1, and frequencies of HSPCs (Lin- Sca1+ cKit +) in the BM Lin- population from Ikaros and/or Helios deleted mice 5 d post-TAM. Lin: CD3, CD4, CD8a, CD11b, CD11c, CD19, B220, Gr1, CD49b, Ter119. **e** Left: representative plots showing CD150 and CD48 expression in HSPCs. Right: frequencies of LT-HSCs (gated as CD150 + CD48-) in HSPCs from 5 d post-TAM. **f** Top: experimental design of competitive BM transplantations. Bottom: representative plots of LT-HSCs from CD45.2 + BM donor cells analyzed 3 mos after TAM-induced deletion in the recipients. Data of healthy animals from 2 independent competitive BM transplantation experiments; *p*-values were calculated with Kruskal-Wallis using Dunn's multiple comparisons test. For c, d and **e**, data were from 9 independent experiments; p-values were calculated with one-way ANOVA using Tukey's multiple comparisons test.

target genes were mapped with the original cell line (WT HPC7) and reciprocal KO cells, deleted for Ikaros or Helios by CRISPR/Cas9-mediated mutagenesis (Fig. 5a), by ChIP-seq. Helios binding in the WT line was previously mapped[19]. In total, 15,710 sites were identified and mapped to 5563 genes. With few exceptions where de novo Ikaros binding was observed in the Helios KO HPC7 cells ($n = 8$; not shown), similar binding profiles were observed for Ikaros and Helios (Fig. 5b and c). Thus, the functional differences between Ikaros and Helios were not due to differences in their DNA binding capacity. We then investigated the transcriptomic changes from bulk mRNA sequencing of primary LT-HSC and MPP3 + 4 (CD48 + CD150- LSK) populations from 5 d post-TAM-treated WT, Ikaros KO, Helios KO and DKO mice. Differentially expressed genes (I Log2 FC I > 1; adj. $p < 0.05$) were then filtered to restrict our analysis to TF-bound genes, using the ChIP-seq data to define the differentially expressed target genes (DETGs).

These analyses revealed that only a few DETGs were identified in the Helios KO LT-HSCs and MPPs compared with WT (Fig. 3a), suggesting that loss of Helios had minimal impact on the expression of most target genes. In contrast, >100-fold more DETGs, mostly upregulated, were found in the Ikaros KO and DKO LT-HSCs and MPPs, indicating that Ikaros loss led to a marked deregulation of the genes bound by these factors. Notably, when the Log2 FC of all the genes deregulated in at least one KO (adj. $p < 0.05$) were plotted together (Fig. 3b), the DETGs up- or downregulated by Ikaros in LT-HSCs were similarly though more weakly deregulated by Helios alone (R = 0.56). Thus, our results suggested that Ikaros and Helios cooperate mainly as transcriptional repressors in LT-HSCs. In contrast, these TFs were both cooperative and antagonistic in MPP3 + 4 cells, especially at lymphoid-related genes, which were downregulated in Ikaros KO but up in Helios KO cells (eg. *Il7r*, *Dntt*, *Rag2* in Fig. 3b). Only one gene, *Wdfy1*, encoding an adaptor protein required for immune complex presentation by follicular DCs[28], was selectively repressed by Helios (Fig. 3b and c).

The effects of Ikaros vs. Ikaros+Helios loss were similar across most DETGs. Upregulated genes in the Ikaros KO LT-HSCs were generally more highly upregulated in the DKO (Fig. 3b), and the overall magnitude of the upregulations was greater than the downregulations. Some genes were uniquely upregulated in the DKO LT-HSCs, (Fig. 3b; *Mpo* in Fig. 3c), suggesting that both Ikaros and Helios were required to repress their expression. Many of these genes encoded proteins important for the lymphoid lineage (eg. *Igll1*, *Pou2af1*, *Il7r*, *Vpreb2*).

We grouped the DETGs into 12 clusters of similarly regulated genes by K-means clustering (Fig. 3d). Most of the clusters contained genes strongly affected by loss of Ikaros or Ikaros+Helios. Two clusters were ectopically induced in both LT-HSCs and MPPs (cluster 1; see also *Cdh5* in Fig. 3c), or only in MPPs (cluster 8; see *Wif1* in Fig. 3c). The other clusters corresponded to genes that were dynamically expressed between WT LT-HSCs and MPPs, but became deregulated in the mutant cells. Clusters 2 and 3 genes were normally expressed in WT LT-HSCs but not MPPs; they were further upregulated in mutant LT-HSCs and MPPs (*Fgd5* in Fig. 3c). Clusters 6 and 7 contained lineage-specific genes that were prematurely expressed in mutant LT-HSCs and MPPs (eg. *Mpo*, *Cebpa*, *Cebpe*, *Il7r*, *Pou2af1*, *Cd14*, *Igll1*, *Tmem119*). Cluster 9 contained genes expressed in WT LT-HSCs and MPPs, but downregulated in the mutant populations, especially the MPPs, while clusters 10 and 11 genes were upregulated between WT LT-HSCs and MPPs, but less efficiently (cluster 10) or not at all (cluster 11) in the mutant MPPs. Finally, cluster 12 comprised genes that were expressed in both WT and mutant LT-HSCs, but were more downregulated in the mutant MP. Ps (*Gfi1b* in Fig. 3c). Given the similarities in gene expression between WT and Helios KO, and the increase in deregulation in the Ikaros KO and DKO samples, we concluded that Ikaros dictates the target gene repertoire, while the combination of Ikaros and Helios is required for greater effect.

Ikaros factors repress the endothelial cell signature in HSPCs

Among the DETGs ectopically expressed in the Ikaros KO and DKO LT-HSCs and MPPs were *Cdh5* (encoding VE-cadherin; CD144), *Tead2* and *Crip2* (clusters 1 and 2 in Fig. 3d), genes not expressed in hematopoietic cells. We therefore screened the upregulated DETGs for non-hematopoietic cell signatures by GSEA. Strikingly, there was a strong enrichment for multiple endothelial cell signatures, with 71 genes upregulated in the Ikaros KO and DKO LT-HSCs (Fig. 4a and b, and not shown). These changes appeared to be long-lasting, as CD144, known for mediating endothelial cell junctions, was expressed by almost all HSPCs and mature lineage-positive cells (Fig. 4c and S6a). Among the upregulated genes were key transcriptional regulators of the endothelial lineage, like *Tead2*, *Crip2* and *Sox18* (Fig. 4d)[29–31]. Signatures of other non-hematopoietic cell types (eg. BM stromal cells, fibroblasts, smooth muscle cells, pericytes), which overlapped with that of endothelial cells (47 of the 71 genes belonged to one of these cell types), were also enriched in the Ikaros KO and DKO LT-HSCs (Fig. 4e). These results suggested that Ikaros and Helios directly repress the expression of endothelial cell markers and regulators in hematopoietic stem and progenitor cells. Indeed, published ATAC-seq data supported the notion that endothelial cell genes (*Flt1*, *Cdh5*, *Crip2*, *Kdr*) were transcriptionally accessible in HSC and MPP populations while epithelial (*Krt9*, *Krt14*) and muscle cell-related (*Myod1*) genes were not (Fig. 6b)[32]. When derepressed upon loss of Ikaros family function, these targets might promote a stable endothelial cell signature in HSPCs and mature hematopoietic cells.

Together with previous findings from our group and others[33–35], the above results suggested that Ikaros factors may prevent cell adhesion in many cell types. We therefore asked if Ikaros repressed the expression of adhesion-related genes both in- and outside of the hematopoietic system. A meta-analysis was performed on available transcriptomic data from Ikaros-deficient HSPCs, preB[36] and naive CD4 + T cells[37], as well as embryonic kidney (HEK293T) cells ectopically expressing Ikaros[38], which identified 45 "core genes" repressed by Ikaros in 3 of the 4 cell types, and 11 genes repressed in all 4 cell types (Fig. 4f). Some of these genes are also expressed in endothelial and other non-hematopoietic cells (eg. *Anxa1*, *Crip2*, *Ifitm2/3*, *Tead2*). The core Ikaros-repressed genes were associated with varied biological pathways such as wounding, cell junction organization, actin cytoskeleton organization, cell migration, and lamellipodium assembly (Fig. 4g). In contrast, only 3 genes downregulated in the absence of Ikaros were detected in 3 out of the 4 cell types (Fig. 6c); none were common to all cells. Thus Ikaros represses a common group of genes involved in cell contact, shape and migration across cell lineages.

https://doi.org/10.1038/s41467-026-78726-z

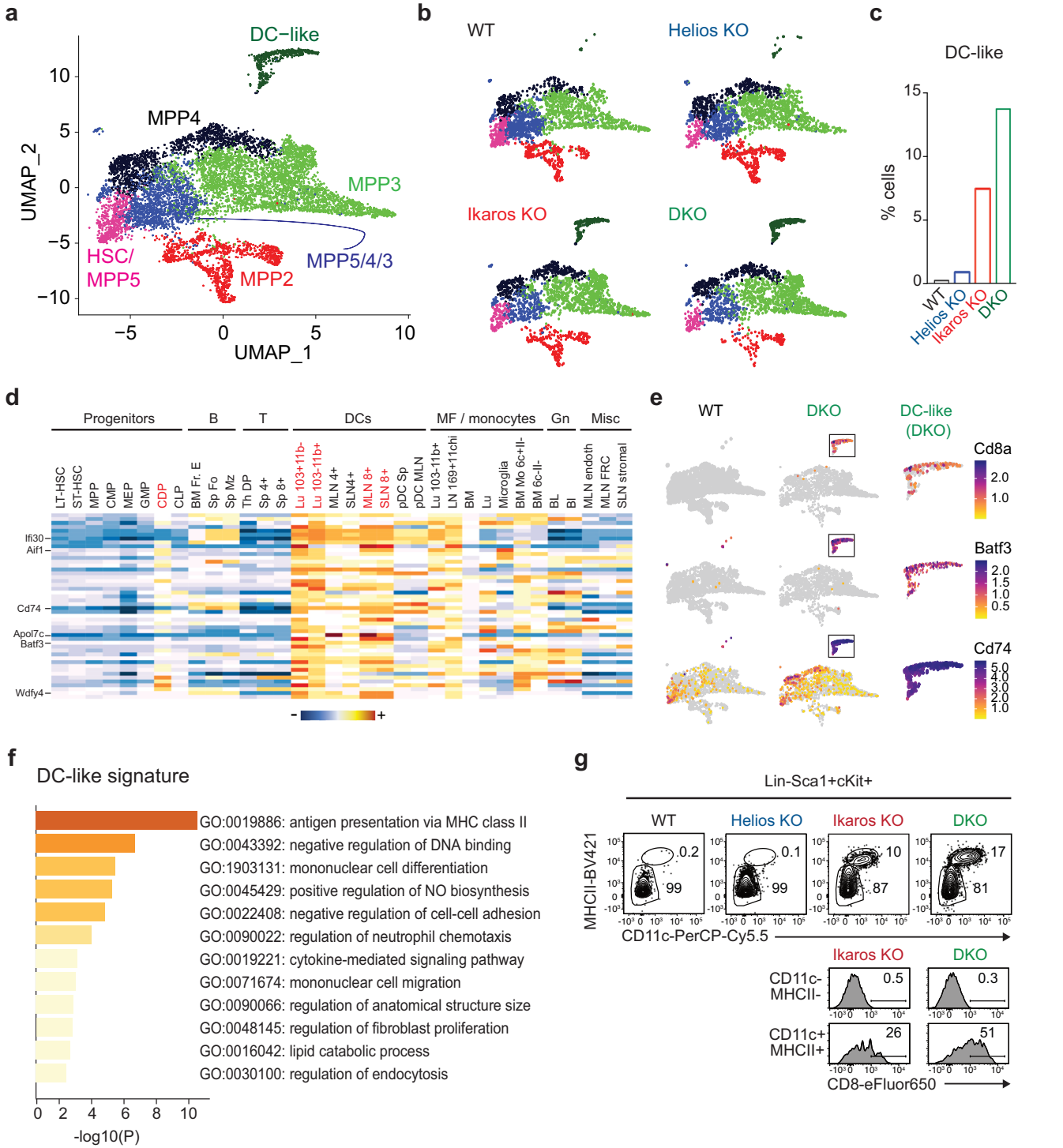


Fig. 2 | Ikaros and Helios repress a DC-like subtype in the HSPC compartment. a, b UMAP plots of combined HSPCs from all mice (**a**), or from the indicated genotypes (**b**; pooled from 2 mice/genotype). **c** Proportion of DC-like cells in HSPCs from the indicated genotypes. **d** Heatmap showing the expression of the top 50 genes overexpressed in the DKO DC-like cells across different cell types (Immgen). Red: DCs or progenitors strongly expressing genes from this signature. **e** WT and DKO HSPCs expressing *Cd8a*, *Batf3,* or *Cd74* from the single cell analysis. **f** Gene ontology (GO) enrichment analysis of the biological pathways associated with the 50 genes defining the DC-like signature. P-values were calculated based on the cumulative hypergeometric distribution. **g** Representative plots of Ikaros and/or Helios KO Lin-Sca1+cKit+ cells expressing MHCII, CD11c, and CD8a, 5 d post-TAM. Lin: CD3, CD4, Ter119, Gr1, CD19, B220, CD49b.

Rapid changes in cell morphology, adhesion and function in Ikaros KO and DKO HSPCs

To assess the immediate biological consequences of Ikaros and/or Helios loss, we deleted the floxed alleles in vitro. Purified HSPCs from untreated WT, Ikaros KO, Helios KO and DKO animals were cultured for 5 days in the presence of 4-hydroxytamoxifen (4OHT) and cytokines (SCF, TPO, IL-3). These conditions allowed us to start with the same HSPC pool across genotypes and avoid potential contamination by endothelial cells. Ikaros and Helios protein levels were well diminished by d5 (Fig. 5a). Loss of Ikaros was already seen at d3 but loss of Helios took longer (not shown). Cells from all samples thrived in these cultures and increased their numbers from the starting

https://doi.org/10.1038/s41467-026-78726-z

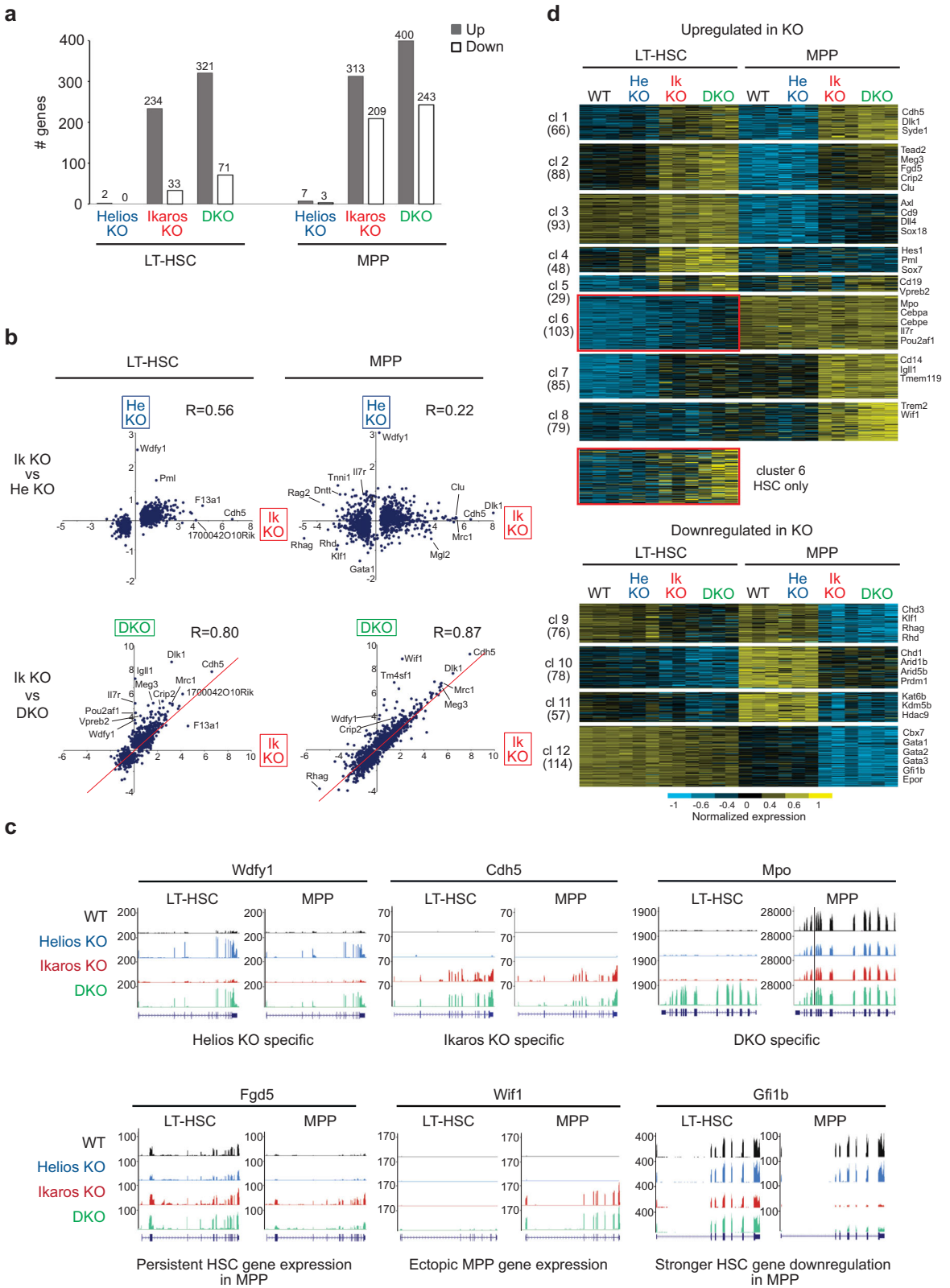
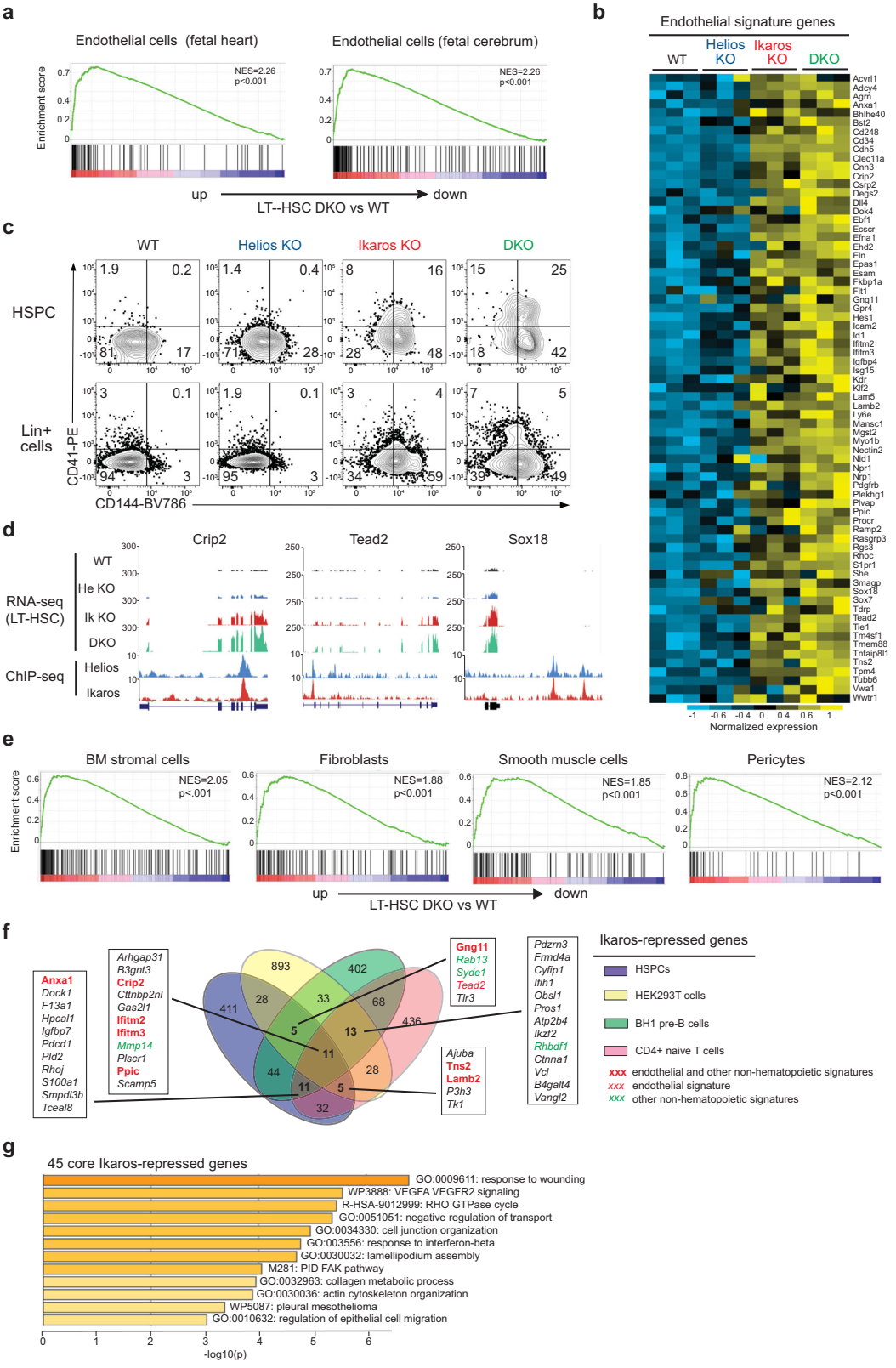


Fig. 3 | Transcriptional impact of Helios and Ikaros loss in HSPCs. a Number of DETGs up- or downregulated in Helios KO, Ikaros KO, and DKO HSPCs, by RNAseq, and restricted to genes identified as bound by Ikaros or Helios by ChIP-seq. Selection criteria were I Log2 FC I > 1; adj. $p < 0.05$. **b** Top: scatter plots showing the Log2 FC of Ikaros KO vs. WT (x-axis) and Helios KO vs. WT (y-axis). Bottom: scatter plots showing the Log2 FC of Ikaros KO vs. WT (x-axis) and DKO vs. WT (y-axis). In all cases, the shown genes correspond to all bound genes found as significantly changed in any of the samples presented in the plot (adj. $p < 0.05$). The red lines in the bottom plots correspond to the diagonal. R is the correlation coefficient. For **a** and **b**, adjusted p-values were calculated using the Benjamini-Hochberg procedure for multiple testings. **c** RNAseq genome browser tracks of differentially regulated genes. **d** K-means clustering ($n = 14$) of genes deregulated in mutant LT-HSCs or MPPs [selection criteria as in (**a**)]. Note that two small clusters with irregular expression patterns across samples are not shown (37 genes). A heatmap comparing the upregulated genes from cluster 6 only in the LT-HSCs is also shown (red boxes).

https://doi.org/10.1038/s41467-026-78726-z



population (Fig. 5b). However, only the Ikaros KO and DKO cultures contained significant numbers of adherent cells that adopted a spindle shape with filopodia development reminiscent of migrating cells (Fig. 5b and c). In ~40% of the mutant cultures between days 5-7, Ikaros KO and DKO cells were observed to self-align into cord-like matrixes that reached 0.4 cm in length, with abundant CD144 positivity between cellular junctions (Fig. 5d and e). Flow cytometry analysis revealed that about one-third of Ikaros KO and DKO cells rapidly acquired CD144-positivity by d5 (Fig. 5f). Thus, Ikaros and Helios directly repress the differentiation of endothelial-like cell structures in HSPCs.

We then evaluated the gene expression programs of mutant non-adherent (na) and adherent (a) HSPCs, by RNA-sequencing of the WT and DKO cultures after 5 days of 4OHT treatment. The DETGs were identified as genes differentially expressed between WT and DKO-na or

Fig. 4 | Upregulation of endothelial and other non-hematopoietic signatures in Ikaros and Helios KO HSCs. a GSEA of two endothelial cell signatures identified among the top-scoring signatures from the GSEA cell signature library upregulated in DKO LT-HSCs. The ranked gene list corresponds to all bound genes detected in the RNA-seq experiment. Normalized enrichment scores (NES) and p-values were estimated using two-sided enrichment analysis with 1,000 permutations. **b** Heatmap of 71 endothelial signature genes upregulated in Ikaros KO and/or DKO HSPCs. Genes were selected when found in at least two distinct endothelial signatures by GSEA. **c** Representative plots of the indicated populations analyzed for CD41 and CD144 expression from mice 5 d post-TAM. **d** RNA- and ChIP-seq genome browser tracks for genes encoding transcription regulators of endothelial cells. The Helios and Ikaros ChIP-seq profiles were obtained from Ikaros KO, and Helios KO HPC7 cells, respectively. **e** GSEA plots showing enrichment of upregulated DKO LT-HSC genes in other non-hematopoietic signatures. NES and p-values were estimated using two-sided enrichment analysis with 1000 permutations. **f** Meta-analysis of genes repressed by Ikaros in four different transcriptomic datasets. HSPCs from the current study; HEK293 cells[38], BH1 preB cells[36] and naive CD4 + T cells[37]. For all datasets, genes were selected to meet the criteria: Log2 FC > 0.5; adj. $p < 0.05$ (for Ikaros KO vs. WT) or Log2 FC < −0.5; adj. $p < 0.05$ (for gain-of-function studies). Adjusted p-values were calculated using the Benjamini-Hochberg procedure for multiple testings. HSPC genes correspond to genes that meet these criteria in both populations. Genes repressed by Ikaros in at least 3 datasets are shown ("core Ikaros-repressed genes"). Genes highlighted in red, green, or bold red belong to the signatures of endothelial cells, other non-hematopoietic signatures (smooth muscle, pericytes, fibroblasts, stromal cells), or both, as indicated (signatures from the GSEA cell type signature library). **g** Pathways associated with the 45 core Ikaros-repressed genes (Metascape). P-values were calculated based on the cumulative hypergeometric distribution.

DKO-a cells, or between DKO-na and DKO-a cells (I Log2 FC I > 1; adj. $p < 0.05$), and restricted to the TF-bound targets. K-means clustering revealed that almost all of the DETGs were deregulated in the same direction between the DKO-na and DKO-a cells; ~80% were upregulated in the DKO-na and -a cells compared with WT (clusters 3 and 4), indicating that they were normally repressed by Ikaros and Helios in WT cells (Fig. 5g). Some DETGs were already enriched in the non-adherent DKO cells (cluster 4), while others were more upregulated in the adherent population (cluster 3), suggesting that the non-adherent DKO cells may represent an intermediate stage. The endothelial cell gene expression program was strongly derepressed in DKO-a and DKO-na cells (Fig. 5h, and not shown for DKO-na cells). Endothelial signature genes like *Cdh5*, *Nid1*, *Tead2*, *Sox18* and *Kdr* were highly upregulated in both the non-adherent and adherent DKO cells (Fig. 5g). In addition, the genes related to the core Ikaros-repressed pathways (cell migration, actin cytoskeleton organization, cell locomotion) were among the upregulated DETGs after in vivo or in vitro deletion (Fig. 4f and g, and S7a). Interestingly, we did not identify genes that were deregulated exclusively in the adherent DKO cells; however, the genes more strongly derepressed in the adherent population were related to inflammation, vasculature development, cell migration, or wound healing (Fig. 7b), indicating a broader response program to injury and tissue repair.

We next asked if other BM-derived progenitor cells, such as mesenchymal stem cells (MSC)[39], were affected by the loss of Ikaros factors. BM cells from 5 d post-TAM-treated single and double KO mice were cultured under MSC-permissive conditions for 4.5 days, and the adherent cells were analyzed for the expression of MSC (CD44) and endothelial cell (CD144) markers (Fig. 8a)[40]. These results showed that the Lin-CD45-CD44+ MSCs arose similarly between the WT and mutant cultures in terms of frequency and cell morphology (Fig. 8b and c), indicating that MSC development did not depend on Ikaros factors. Importantly, the MSCs did not express CD144, suggesting that the mutant MSCs did not become endothelial-like cells in these conditions. Thus, HSPCs have the potential to activate an endothelial cell program in the absence of Ikaros factors.

To determine if WT HSPCs could spontaneously acquire endothelial-like features, we stressed them in culture for 8 days in the same medium, as hematopoietic cells have been reported to transform into endothelial-like cells during inflammation, angiogenesis, or in the presence of angiogenic growth factors[4,41–43]. Strikingly, some WT cells became adherent, and cord-like structures were observed in about 40% of the cultures (Fig. 6a), like those seen in DKO cells. Notably, WT HSPCs spontaneously lost Ikaros and Helios expression in these conditions (Fig. 6b). These results suggested that Ikaros family TFs can be downregulated in WT HSPCs upon stress, allowing these cells to undergo endothelial cell-like differentiation.

Lastly, we evaluated whether the newly differentiated endothelial-like cells were functional by measuring their ability to transcytose low-density lipoproteins (LDL), a basic function of the endothelial cell barrier that modulates circulatory lipid uptake. HSPCs from untreated WT, Ikaros KO and DKO BM cells were cultured in the presence of 4OHT, cytokines and serum for 5 or 8 (stressed WT condition) days, then rested in the absence of serum, and incubated with acetylated (Ac)-LDL (Fig. 6c). These results revealed that the mutant and stressed WT HSPCs incorporated elevated levels of Ac-LDL, with the highest levels observed in the DKO cells, while fewer WT cells were Ac-LDL^{hi}.

Altogether, our results indicated that HSPCs acquired endothelial cell morphology and function upon loss of Ikaros and Helios.

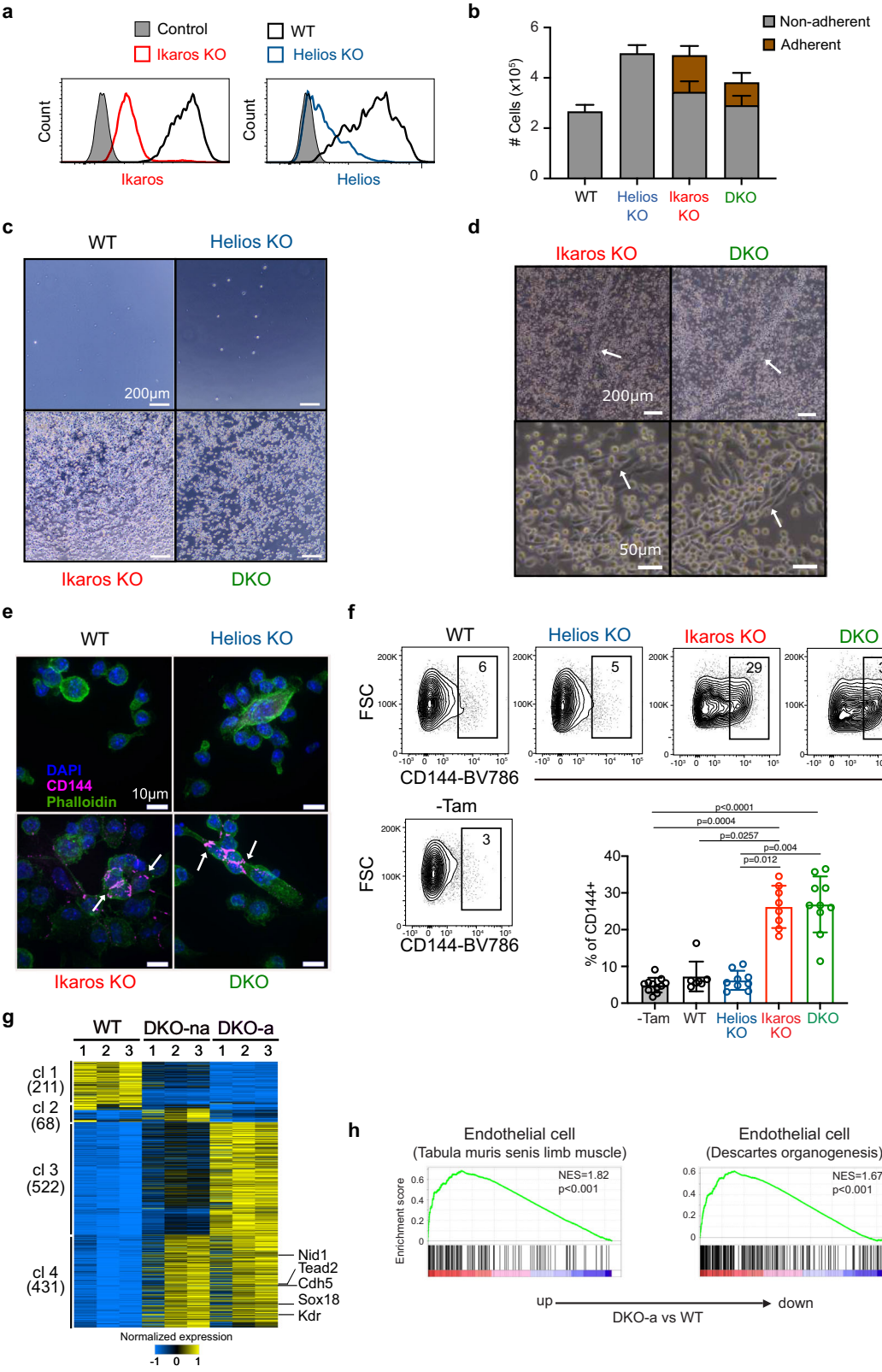
Discussion

We show here that Ikaros and Helios are major regulators of HSPC identity in the adult bone marrow. Within days of in vivo deletion, mutant LT-HSCs and MPPs exhibit a derepression of Ikaros target genes normally observed in mature hematopoietic cells, like those encoding lineage-affiliated transcriptional regulators and effector molecules. The most obvious example is the appearance of CD8 + DC-like cells with antigen-presenting characteristics within the HSPCs. Further, loss of Ikaros, alone or in combination with Helios, results in derepression of genes associated with non-hematopoietic cells, notably those of the endothelial lineage. Indeed, endothelial-like cells arise within 24 h of TF loss, either by depleting the floxed alleles in mutant cells, or through stress of WT cells that was accompanied by a subsequent downregulation of Ikaros and Helios. Importantly, Ikaros-deficient LT-HSCs still express HSC-related genes. Thus, Ikaros factors are not required for LT-HSC determination but are instead required to maintain LT-HSC identity by repressing promiscuous target gene expression.

A potential caveat of in vivo deletion is the risk of contaminating mature hematopoietic and non-hematopoietic cells in our analyses. We excluded this possibility by deleting the floxed alleles in vitro. This allowed us to compare cultures from the same starting HSPCs, and demonstrate that only the in vitro-deleted cells become adherent and form cord-like structures after deletion. Further, the adherent cells still express HSPC-associated markers like cKit and Sca1, unlike bona fide endothelial cells. We therefore conclude that the endothelial-like cells arose from bona fide HSPCs. Whether the endothelial-like cells arise from LT-HSCs or MPPs remains an open question, as both populations ectopically express endothelial lineage genes after deletion. Our data suggest that a subset of the endothelial-like cells might also be DC-like, and vice versa. RNA-sequencing and surface marker analyses of the in vitro-deleted adherent and non-adherent cells show high levels of mRNA and protein for CD11c and MHC class II molecules (G.B., unpublished results). Conversely, the DC-like cells also express CD144. These results indicate that the newly developed lineage-positive hematopoietic and non-hematopoietic cells show traces of their HSPC ancestry even as they activate genes and pathways consistent with effector function.

Another hazard of in vivo deletion with inducible or tissue-specific mouse lines is the transient inflammation associated with Cre activity,

https://doi.org/10.1038/s41467-026-78726-z



as seen in the HSPC compartment of Cre+ (+/+ Cre +) control animals compared with Cre- (f/f Cre-) mice. To address this caveat, we analyzed HSPCs deleted after transplantation, when inflammation was minimal, and donor Ikaros KO and DKO LT-HSCs were similarly lost. Further, germline-deleted LT-HSCs were also absent in the Ikaros KO and DKO fetal livers, where the Cre recombinase was never introduced. Thus, several experimental systems support a direct role for Ikaros factors in LT-HSC maintenance.

Ikaros and Helios bind DNA with nearly identical profiles but Ikaros and Ikaros+Helios have a stronger effect on gene expression than Helios alone. The reason for this is unclear. Ikaros and Helios have been shown to bind DNA as homo- and heterodimers in lymphocytes. If similar dimer combinations exist in HSPCs, then our results suggest

Fig. 5 | In vitro deletion of Ikaros and/or Helios in HSPCs causes rapid changes in cell morphology and adhesive properties. a Loss of Ikaros and Helios in HSPCs from Ikaros or Helios floxed cells after 5 d of 4OHT treatment in culture in the presence of SCF, TPO, and IL-3. The control staining corresponds to secondary antibody staining of pooled WT and KO cells. **b** Numbers of non-adherent and adherent cells after 5 d in 4OHT, starting from 5×10^3 cells. Data from 3 independent experiments. Mean ± SD are shown. **c** Phase contrast microscopic images (x10) showing the adherent cells seen after washing of the indicated cultures after 5 d in 4OHT. Images are representative of 24 independent experiments. **d** Phase contrast microscopic images (x10 top, x40 bottom) of Ikaros KO and DKO cultures after 5–7 d of 4OHT culture (medium changed at d5). Arrows indicate the presence of spindle-shaped cells aligned in linear patterns in the Ikaros KO and DKO adherent cells seen after washing. Images are representative of 10 out of 24 independent experiments. **e** Confocal fluorescence microscopic images (x100) of HSPCs stained for CD144, F-actin (phalloidin) and DNA (DAPI). White arrows indicate junctional localization of CD144. Representative of >3 independent experiments. **f** Top: representative plots of CD144 expression of 5 d 4OHT cultures of the indicated HSPCs. Bottom: frequencies of CD144+ cells from the indicated cultures. "-TAM" corresponds to DKO HSPCs cultured for 5 d in the absence of 4OHT. Data were from 8 independent experiments. Mean ± SD are shown. P-values were calculated with Kruskal-Wallis using Dunn's mutiple comparisons test. **g** K-means clustering ($n = 4$) of bound genes differentially expressed in WT, DKO-na and DKO-a HSPCs (| Log2 FC | ≥1; adj. $p \leq 0.01$). Adjusted p-values were calculated using the Benjamini-Hochberg procedure for multiple testings. **h** GSEA of endothelial cell signatures that were among the top scoring signatures from the GSEA cell signature library and upregulated in DKO-a HSPCs. The ranked gene list corresponds to all genes that were detected in the RNA-seq experiment. NES and p-values were estimated using two-sided enrichment analysis with 1000 permutations.

that the Ikaros homodimers and Ikaros-Helios heterodimers co-repress most of the target genes in these cells, which would explain why the dominant-negative Ikaros mutation has a greater effect on LT-HSC function than the Ikaros null one[18]. Further, Ikaros represses a core group of 45 target genes that promote cell contact, shape and migration in numerous cell types, including cells that do not normally express this factor, in line with the important function of Ikaros as an anti-adhesion regulator[38]. The one notable exception is a group of lymphoid-related target genes that is activated by Ikaros but repressed by Helios (Fig. 3b). Repression of these lymphoid genes by Helios may be why this factor is downregulated during lymphoid commitment in CLP cells (Fig. 1a and ref. 44).

Our results indicate that adult HSPCs retain a high level of cellular plasticity. Earlier studies had suggested that HSCs can respond to tissue damage or transplantation by transdifferentiating into non-hematopoietic cells like myocytes, neurons, and endothelial cells[5,42,43,45–47], though these findings were tempered after data re-analysis suggested that the HSC populations were contaminated with non-hematopoietic precursor cells[48]. More recently, a small percentage of human peripheral blood CD34+ HSCs were reported to develop into CD144+ spindle-shaped cells after about 1 month in culture in the presence of vascular endothelial growth factor (VEGF)[43], suggesting that HSCs can differentiate towards the endothelial lineage through an unknown mechanism. Our findings that HSPCs develop into endothelial-like cells one day after Ikaros loss, in the absence of VEGF, uncover a molecular mechanism by which Ikaros and Helios act as potent negative regulators of cellular plasticity.

Why do Ikaros-deficient HSPCs develop into endothelial-like cells and not other non-hematopoietic cell types? One simple explanation may be the close developmental relationship between hematopoietic and endothelial cells[49]. The first definitive HSPCs arise from endothelial precursors during embryogenesis via a highly conserved process called the endothelial-to-hematopoietic transition (EHT). This transition involves the activation of a hematopoietic transcriptional program in a proportion of endothelial cells which then become hemogenic and go through major morphological changes to adopt a hematopoietic cell fate[49,50]. Indeed, upregulation of Ikaros and Helios was detected in yolk sac and the aorta-gonad-mesonephros pre-hemogenic and hemogenic endothelial cells by scRNA-sequencing, suggesting that these factors could repress the endothelial program during EHT[51]. Adult HSPCs may retain an epigenetic memory of the endothelial lineage by maintaining endothelial genes in a poised state. Ikaros may be implicated in this process through its modulation of epigenetic marks[17].

Lastly, our results indicate that WT HSPCs can rapidly become endothelial-like cells under stress, a transition that correlates with the downregulation of Ikaros and Helios. As HSPCs circulate in human peripheral blood and have been reported to transform into endothelial-like cells in vivo, it may be important to consider that Ikaros and Helios can be transiently and selectively degraded using available immunomodulatory imide drugs[52–54], especially during critical situations that may require wound healing or de novo vasculogenesis.

Methods

Mice

The *Ikzf1* floxed, *Ikzf2* null, and R26-CreERT2 (Cre) knock-in alleles, were previously described[36,55,56]. The *Ikzf1* null mouse line was generated by crossing *Ikzf1*$^{f/f}$ mice with deleter Tg(CMV-Cre)1Ipc animals[57]. The *Ikzf2*$^{f/f}$ line was generated by inserting loxP sites upstream of exon 8 and downstream of the stop codon within exon 8, by homologous recombination in ES cells. *Ikzf1* and *Ikzf2* null mice were kept on a mixed 129/Sv: C57BL/6 background, while the *Ikzf1*$^{f/f}$ and *Ikzf2*$^{f/f}$ R26-CreERT2+ mice were on the C57BL/6 background. Mice were injected intraperitoneally (i.p.) with 75 mg/kg of TAM for five consecutive days to induce deletion of the floxed alleles. All mice were bred and maintained in a specific pathogen-free (SPF) facility and used according to IGBMC Ethical Committee (Com'Eth) guidelines. Blood cell counts were performed on an Advia 120 (Siemens AG) with the Veterinary software. Animal experiments were approved by the ethical section of the French Ministry of Research and Innovation with the approval numbers: APAFIS 28424-202011261221575 4v3, 48088-202401301459435v5 and 49308-2024219917089109v5. For all experiments, both female and male mice (12-20 weeks of age) were included and evenly distributed across the experimental groups.

Flow cytometry and cell sorting

Cells were stained with the antibody (Ab) combinations listed in Table S2 in PBS/1% FCS. Samples were acquired on a Fortessa X20 analyzer (BD Biosciences) and analyzed with the FlowJo 10 software. For intracellular staining, cells were fixed and permeabilized using the eBioscience Foxp3/Transcription Factor Staining Kit (Invitrogen), then stained with the primary Ab for 1 h at room temperature (RT) or overnight (ON) at 4 °C when necessary and with a secondary Ab for 1 h at RT. For cell cycle staining, Ki67 was added after cell fixation and incubated for 30 min on ice. DAPI (1 µg/ml Invitrogen) was added and samples were acquired within 10 min. For sorting HSPCs and HSPC subsets, cells were stained for lineage marker expression before depletion with Dynabeads sheep anti-rat IgG beads (Invitrogen). Lineage-negative cells were stained as above and sorted in the presence of DAPI on a FACS Fusion (BD Biosciences). Sort purity was >95%. Gating strategies for the analyses and sorts are shown in Fig. S9.

BM competitive transplantation assays

5×10^5 WT or Ikzf1$^{f/f}$ and/or Ikzf2$^{f/f}$ Cre+ BM cells from CD45.2+ mice were intravenously (i.v.) injected with 5×10^5 CD45.1 + WT BM cells into 9 Gy lethally-irradiated CD45.1 + CD45.2+ hosts. Peripheral blood (PB) was analyzed 1 month after reconstitution, as described previously[58]. Mice with comparable PB reconstitution of CD45.1+ and CD45.2+ cells were injected i.p. daily for 5 days at 75 mg/kg TAM. PB was analyzed 1,

https://doi.org/10.1038/s41467-026-78726-z

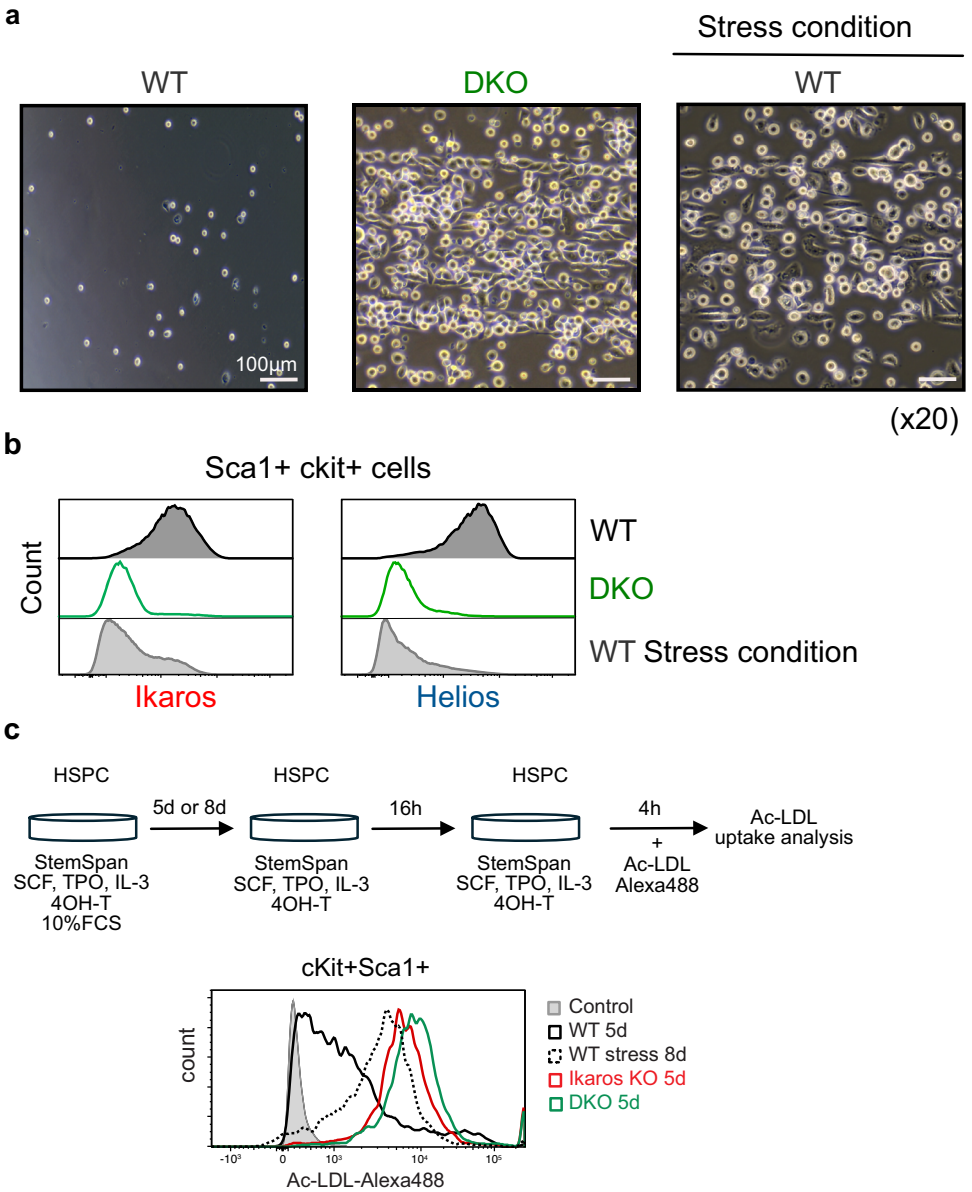


Fig. 6 | Increased cell adhesion and loss of Ikaros and Helios expression in WT HSPCs cultured under stress conditions. a Phase contrast microscopic images (x20) of WT HSPCs cultured under normal or stressed conditions (8 d) and DKO HSPCs under normal conditions (4OHT, 8 d). Images correspond to adherent cells seen after washing. Stress-induced linear cell alignment and spindle-shaped morphology of the WT HSPCs were similar to those observed with DKO HSPCs ($n = 5$). **b** Expression of Ikaros and Helios in the indicated cells, as measured by flow cytometry. **c**) Representative Ac-LDL uptake by the indicated HSPCs. All samples were cultured for 5 d, except for the stressed WT condition, which was cultured for 8 d ($n = 2$).

2, and 3 months after injection. BM was analyzed after 3 mos of gene deletion, and CD45.2+ HPSCs were analyzed by flow cytometry.

Single-cell mRNA seq

Single-cell mRNA sequencing was performed on the 10X Genomics platform using the 3' mRNA Single Cell Library Preparation Kit (10x Genomics) following the manufacturer's instructions. 15- to 20-week-old male WT (*Ikzf1*$^{+/+}$ *Ikzf2*$^{+/+}$ Cre +), Ikaros KO (*Ikzf1*$^{f/f}$ Cre +), Helios KO (*Ikzf2*$^{f/f}$ Cre +) and DKO (*Ikzf1*$^{f/f}$ *Ikzf2*$^{f/f}$ Cre +) mice were injected i.p. with TAM every day for 5 d followed by 5 d of rest. 10^5 HSPCs were sorted into PBS/0.4% BSA. HSPCs were pooled from two mice per genotype after sorting. The cell viability was >80% for all samples. Cells were loaded into a Chromium Controller (10x Genomics) according to the manufacturer's instructions, aiming for a targeted cell recovery of 5×10^3 cells. The quality of the obtained cDNA library upon adapter ligation and index PCR was assessed by Bioanalyzer fragment analysis (HS DNA Kit, Agilent). Sequencing was performed on HighSeq 2000 (Illumina).

The 3' mRNA-seq reads were mapped against the mm10 reference genome. STARsolo was used to map, deduplicate and count reads to create BAM files and the Seurat object containing the gene counts[59]. The data quality was assessed using DeeptoolsQC. After preprocessing, the analysis of single-cell RNA-seq data was performed using the R package Seurat[60]. Cell filtering was performed and cells containing <1000 or >6000 genes were excluded from the analysis to avoid doublets or empty droplets. Poor-quality or dying cells with >10% mitochondrial gene contamination were also excluded. Data were normalized, and integration was performed. Data were then scaled and linear dimensional reduction with the Principal Component Analysis (PCA) was applied. After applying the JackStraw and Elbow plot procedures from Seurat, a clustering analysis was performed selecting the first 20 PCs, resulting in 16 clusters which were visualized using the

Uniform Manifold Approximation and Projection (UMAP). After additional filtering, using previously published Lin- Sca1+ cKit+ and Lin- Sca1- cKit+ signatures[61], two clusters were removed. Gene signature scores were computed with Seurat's AddModuleScore function using log-normalized expression values, generated after library-size normalization and log-transformation. The resulting scores represent relative enrichment of the signature genes in each cell, normalized against matched control genes with comparable expression levels. The enrichment of the HSC/MPP1/2/3/4/5 signatures previously published[26] was used for annotation. Clusters sharing the same annotation were grouped together, identifying 6 differentially annotated cell clusters that were further analyzed.

Transcriptome analysis by RNA-seq

Total RNA was extracted from $0.7–4 \times 10^4$ LT-HSCs (LSK CD150 + CD48-) and $0.7–3.5 \times 10^5$ MPPs (LSK CD150- CD48 +) from WT and KO mice or from $3\text{-}4 \times 10^5$ WT and DKO non-adherent and adherent HSPCs from culture (three samples per group) using the RNeasy Plus Micro Kit (Qiagen). Libraries were prepared with the Takara SMART-seq v4 Ultra Low Input RNA Kit, followed by the Illumina Nextera XT DNA sample preparation kit, and sequenced with a NextSeq 2000 (Illumina) with single-end 50 bp reads. Reads were preprocessed to remove adapters, poly(A), and low-quality sequences (Phred quality score below 20) using Cutadapt version 1.10. Reads shorter than 40 bases were discarded for further analysis. Reads were aligned to the *M. musculus* genome mm10 using STAR v2.5.3a. Gene expression quantification was performed from uniquely aligned reads using htseq-count (v0.6.1p1), with annotations from ENSEMBL GRCm38. Differential gene expression analyses were performed using the Bioconductor package DESeq2 (v1.16.1). Differentially expressed genes were selected according to the following criteria: I log2 FoldChange I > 1; adj. $p < 0.05$. Heatmaps of differentially expressed genes were created using Gene Cluster v3.0 and the Java TreeView software for HSCs and MPPs, and Morpheus (https://software.broadinstitute.org/morpheus) for HSPC in culture. For GSEA, the FCs of all genes detected in the RNA-seq experiments were used to generate the ranked gene lists. The different cell signatures were taken from the GSEA cell signature library. Gene ontology enrichment analysis was performed using Metascape[62].

HPC7 cells

The HPC7 cell line was cultured in IMDM supplemented with 5% FCS, penicillin/streptomycin, monothioglycerol (150 µM; Merck), mSCF (100 ng/ml; Peprotech), and mIL-6 (10 ng/ml, Peprotech)[27]. HPC7 cells were plated at 1.5×10^5 cells/ml and split every 2-3 days. To delete Ikaros and Helios using the CRISPR-Cas9 technique, HPC7 cells were electroporated with two ribonucleoprotein (RNP)-sgRNA complexes produced as indicated in Table S3. The sgRNA (44µM) was prepared by incubating the designed crRNA (targeting *Ikzf1* and *Ikzf2* exon 8 and listed in Table S3) with a tracrRNA (both provided from IDT) in Nuclease free TE Buffer at 95 °C for 5 min. To prepare the RNP-sgRNA complexes, the produced sgRNA (Cf=22 µM) were incubated with HiFi Cas9 (IDT) at RT for 15 min. The prepared RNP-sgRNA complexes were diluted in an electroporation mix containing also an Electroporation Enhancer (Cf=2,16 µM) and 500 ng of pMIG vector (as transfection control). 10^6 HPC7 were resuspended in 10 µl of electroporation mix and electroporated using the 10 µl tip of a Neon™ NxT Electroporation System (ThermoFisher) and the following settings: pulse voltage 1500 V, pulse width 20 ms, pulse number 1. After electroporation, cells were resuspended in 500 µl of medium (without penicillin/streptomycin) in 24-well plates. 24 h after transfection, HPC7 cells were harvested and stained with HSPC cell markers. HSPC GFP + HPC7 cells were cloned and cultured in 96-well plates containing 50 µl of complete medium. Cells were expanded and screened for Ikaros and Helios deletion by PCR, using the genotyping primers in Table S3. The Ikaros KO and Helios KO clones were further expanded and deletion was confirmed by intracellular staining using flow cytometry.

ChIP-seq

The ChIP-sequencing experiments were performed as described previously[19]. 2 independent ChIP-seq experiments were performed with the Ikaros antibody[63] in WT and Helios KO HPC7 cells (with 2 independent KO clones); 3 independent ChIP-seq experiments were performed with the Helios antibody (Cell Signaling) in Ikaros KO HPC7 cells (3 independent KO clones). 50×10^6 HPC7 cells were harvested and washed with PBS. Protein-DNA cross-linking was achieved by incubating cells in 1% PFA for 10 min at RT, and the reaction was quenched with glycine (133 mM final) for 5 min. Cell lysis was performed in prechilled LB2 buffer (10 mM Tris-HCl pH 8, 1 mM EDTA, 0.5 mM EGTA, and 200 mM NaCl) in the presence of a protease inhibitor cocktail (Roche) for 10 min at 4 °C. The obtained nuclei were resuspended in LB2.3 (18 mM Tris-HCl pH 8, 1 mM EDTA, 0.5 mM EGTA, 200 mM NaCl, 0.033% Na-deoxycholate, and 0.16% N-laurylsarcosine) and sonicated for five cycles (5 min high, 15 s on/15 s off) with a Bioruptor sonicator (Diagenode). The sonicated chromatin was 10x diluted (50 mM Tris-HCl pH 8, 200 mM NaCl, 5 mM EDTA, 0.5% NP-40), precleared for 1 h at 4 °C, and incubated ON at 4 °C with an anti-Ikaros rabbit polyclonal (against the Ikaros C-terminus, produced in-house) or anti-Helios rabbit monoclonal (Cell Signaling) Ab. Immunoprecipitation (IP) was carried out for 1 h at 4 °C using protein A-Sepharose beads (Sigma-Aldrich) in the presence of 0.1% SDS, followed by six washes in washing buffer (20 mM Tris-HCl pH 8, 500 mM NaCl, 2 mM EDTA, 1% NP-40, 0.1% SDS) and three in 10 mM Tris-HCl pH 8, 1 mM EDTA. The elution of the IP-ed complexes was done in 2% SDS in 10 mM Tris-HCl pH 8, 1 mM EDTA for 1 min at RT. De-crosslinking was performed in the elution buffer ON at 65°C, whereas the input chromatin was decrosslinked in 200 mM NaCl under the same conditions. DNA was purified using the MinElute PCR Purification Kit (Qiagen). Libraries were prepared using the MicroPlex Library Preparation Kit v2 (Diagenode) following the manufacturer's instructions. Single-end 50 bp sequences were obtained with the HiSeq4000.

Image analysis and base calling were performed by using RTA 2.7.7 and bcl2fastq 2.17.1.14. Adapter dimer reads were removed using Dimer Remover (https://sourceforge.net/projects/dimerremover/). Read alignment was performed to mm10 mouse genome using Bowtie. Peak calling was performed using MACS2 v2.2.7[64] with relaxed p-value threshold (0.01) and maximal peak half-width of 200 bp. Irreproducible Discovery Rate software (IDR) was used to identify reproducible peaks between replicates, using default parameters and IDR threshold ≤0.05[65]. Peaks were annotated using ChIPseeker 1.28.3[66]. To find the regions differentially bound by Ikaros and Helios in WT and KO HPC7 cells, we used the R Bioconductor package DiffBind[67] with default parameters. Data were visualized using the UCSC Genome Browser. Heatmaps were generated using Deeptools v3.5. The tool computeMatrix was used to generate a count matrix at the reference positions of interest, and the tool plotHeatmap was used to generate heatmaps.

HSPC and MSC cultures

HSPCs were isolated from BM by FACS as described below. Sorted cells were cultured in 24-well culture plates at 5×10^3 cells/ml in StemSpan™ SFEM medium (StemCell Technologies), supplemented with 10% FCS, gentamicin, penicillin/streptomycin, and the recombinant murine cytokines from Peprotech: SCF (10 ng/ml), TPO (100 ng/ml), IL-3 (10 ng/ml). Gene deletion of *Ikzf1* and/or *Ikzf2* was achieved by the addition of 100 nM 4OHT to the culture medium. Cells were incubated for 5 d at 37 °C, under 5% CO_2 in a humid atmosphere. Non-adherent cells were collected with 3x washes with PBS/1% FCS and adherent cells by mechanical cell scraping. Adherent cells in the wells were observed with phase contrast under an optical microscope (EVOS). In stressed

conditions, HSPCs were cultured in 6-well plates for 8 d; for HSPC cultures without stress, the medium was changed 5 d after culture initiation. For immunostaining, HSPCs were grown on LabTek II chamber slides (Nunc) for 5 d. Cells were fixed with 4% PFA/PBS without Ca++ or Mg++ for 10 min at RT. After washing 3x with PBS, cells were permeabilized for 10 min with 0.3% Triton/PBS and blocked for 30 min with 10% rat serum in PBS at RT. Cells were stained ON at 4 °C with an anti-VE-Cadherin-APC Ab diluted 1/100 (BioLegend). After 3x PBS washes, actin filament staining was performed with Alexa Fluor 488-conjugated phalloidin (Santa Cruz) diluted 1/400 for 30 min at RT. The culture chambers were then removed, and coverslips were mounted on slides with Fluoromount-G with DAPI (Invitrogen). Images were collected using a Nikon CSU-X1 Spinning-Disk microscope and processed using Fiji software. For the Ac-LDL uptake assays, HSPCs were cultured as above for 5 d or 8 d (stressed WT condition), then rested for 16 h in medium without FCS, and incubated with Alexa-488-conjugated AcLDL (#L23380, Invitrogen) for 4 h at 37 °C, followed by flow cytometric analysis[68]. For the MSC cultures, total BM cells were cultured in 10 ml of DMEM, 15% FCS, gentamicin, penicillin/streptomycin and 2 mM glutamine. Non-adherent cells were removed after 36 h by changing the media. After 3 days of culture, MSCs were analyzed by phase-contrast microscopy and flow cytometry[40].

Reporting summary

Further information on research design is available in the Nature Portfolio Reporting Summary linked to this article.

Data availability

A Source data file containing the numerical values used in graphs is provided as supplementary material. Publicly available datasets and databases used in this study included: GSE51350[36], GSE157813[37] and KAP230738[38]. ChIP-seq and RNA-seq data have been submitted to the NCBI data base and are available under the accession numbers GSE306060, GSE306061, GSE306120 and GSE309209. Processed RNA-seq data are provided in Supplementary Data 1. Source data are provided with this paper.

References

1. Haas, S., Trumpp, A. & Milsom, M. D. Causes and consequences of hematopoietic stem cell heterogeneity. *Cell Stem Cell* **22**, 627–638 (2018).
2. Wang, Z. & Ema, H. Mechanisms of self-renewal in hematopoietic stem cells. *Int J. Hematol.* **103**, 498–509 (2016).
3. Purton, L. E. Adult murine hematopoietic stem cells and progenitors: an update on their identities, functions, and assays. *Exp. Hematol.* **116**, 1–14 (2022).
4. Toth, Z. E. et al. The combination of granulocyte colony-stimulating factor and stem cell factor significantly increases the number of bone marrow-derived endothelial cells in brains of mice following cerebral ischemia. *Blood* **111**, 5544–5552 (2008).
5. Plein, A., Fantin, A., Denti, L., Pollard, J. W. & Ruhrberg, C. Erythromyeloid progenitors contribute endothelial cells to blood vessels. *Nature* **562**, 223–228 (2018).
6. Zipori, D. Blood to brain yet again. *Blood* **111**, 5422–5423 (2008).
7. Barcia Duran, J. G., Lis, R. & Rafii, S. Haematopoietic stem cell reprogramming and the hope for a universal blood product. *FEBS Lett.* **593**, 3253–3265 (2019).
8. John, L. B. & Ward, A. C. The Ikaros gene family: transcriptional regulators of hematopoiesis and immunity. *Mol. Immunol.* **48**, 1272–1278 (2011).
9. Heizmann, B., Kastner, P. & Chan, S. The Ikaros family in lymphocyte development. *Curr. Opin. Immunol.* **51**, 14–23 (2018).
10. Molnar, A. & Georgopoulos, K. The Ikaros gene encodes a family of functionally diverse zinc finger DNA-binding proteins. *Mol. Cell Biol.* **14**, 8292–8303 (1994).
11. Sun, L., Liu, A. & Georgopoulos, K. Zinc finger-mediated protein interactions modulate Ikaros activity, a molecular control of lymphocyte development. *EMBO J.* **15**, 5358–5369 (1996).
12. Payne, M. A. Zinc finger structure-function in Ikaros Marvin A Payne. *World J. Biol. Chem.* **2**, 161–166 (2011).
13. Gounari, F. & Kee, B. L. Fingerprinting ikaros. *Nat. Immunol.* **14**, 1034–1035 (2013).
14. McCarty, A. S., Kleiger, G., Eisenberg, D. & Smale, S. T. Selective dimerization of a C2H2 zinc finger subfamily. *Mol. Cell* **11**, 459–470 (2003).
15. Affar, M. et al. IKAROS: from chromatin organization to transcriptional elongation control. *Cell Death Differ.* **32**, 37–55 (2025).
16. O'Neill, D. W. et al. An ikaros-containing chromatin-remodeling complex in adult-type erythroid cells. *Mol. Cell Biol.* **20**, 7572–7582 (2000).
17. Oravecz, A. et al. Ikaros mediates gene silencing in T cells through Polycomb repressive complex 2. *Nat. Commun.* **6**, 8823 (2015).
18. Nichogiannopoulou, A., Trevisan, M., Neben, S., Friedrich, C. & Georgopoulos, K. Defects in hemopoietic stem cell activity in Ikaros mutant mice. *J. Exp. Med* **190**, 1201–1214 (1999).
19. Cova, G. et al. Helios represses megakaryocyte priming in hematopoietic stem and progenitor cells. *J. Exp. Med.* **218**, 10.1084/jem.20202317 (2021).
20. Loonstra, A. et al. Growth inhibition and DNA damage induced by Cre recombinase in mammalian cells. *Proc. Natl. Acad. Sci. USA* **98**, 9209–9214 (2001).
21. Higashi, A. Y. et al. Direct hematological toxicity and illegitimate chromosomal recombination caused by the systemic activation of CreERT2. *J. Immunol.* **182**, 5633–5640 (2009).
22. Papathanasiou, P. et al. Self-renewal of the long-term reconstituting subset of hematopoietic stem cells is regulated by Ikaros. *Stem Cells* **27**, 3082–3092 (2009).
23. Winandy, S., Wu, P. & Georgopoulos, K. A dominant mutation in the Ikaros gene leads to rapid development of leukemia and lymphoma. *Cell* **83**, 289–299 (1995).
24. Dumortier, A. et al. Notch activation is an early and critical event during T-Cell leukemogenesis in Ikaros-deficient mice. *Mol. Cell Biol.* **26**, 209–220 (2006).
25. Kastner, P. Chan S. Role of Ikaros in T-cell acute lymphoblastic leukemia. *World J. Biol. Chem.* **2**, 108–114 (2011).
26. Sommerkamp, P. et al. Mouse multipotent progenitor 5 cells are located at the interphase between hematopoietic stem and progenitor cells. *Blood* **137**, 3218–3224 (2021).
27. Pinto do, O. P., Kolterud, A. & Carlsson, L. Expression of the LIM-homeobox gene LH2 generates immortalized steel factor-dependent multipotent hematopoietic precursors. *EMBO J.* **17**, 5744–5756 (1998).
28. Zhen, Y. & Shao, W. H. WDFY1-expressing follicular dendritic cells play a critical role in lupus development in cGVHD mouse model. *J. Immunol.* **214**, 1160–1172 (2025).
29. Yoo, H. B. et al. A TEAD2-Driven Endothelial-Like Program Shapes Basal-Like Differentiation and Metastasis of Pancreatic Cancer. *Gastroenterology* **165**, 133–148 e117 (2023).
30. Yang, S., Zhang, X., Li, X. & Li, H. Crip2 affects vascular development by fine-tuning endothelial cell aggregation and proliferation. *Cell Mol. Life Sci.* **82**, 110 (2025).
31. Zhou, Y., Williams, J., Smallwood, P. M. & Nathans, J. Sox7, Sox17, and Sox18 Cooperatively Regulate Vascular Development in the Mouse Retina. *PLoS One* **10**, e0143650 (2015).
32. Itokawa, N. et al. Epigenetic traits inscribed in chromatin accessibility in aged hematopoietic stem cells. *Nat. Commun.* **13**, 2691 (2022).
33. Deau M-C, et al. How Ikaros and Aiolos homo- and heterodimers drive gene expression to ensure B cell development. *bioRxiv*, 2025.2006.2009.658591 (2025).

34. Joshi, I. et al. Loss of Ikaros DNA-binding function confers integrin-dependent survival on pre-B cells and progression to acute lymphoblastic leukemia. *Nat. Immunol.* **15**, 294–304 (2014).
35. Hu, Y. et al. Superenhancer reprogramming drives a B-cell-epithelial transition and high-risk leukemia. *Genes Dev.* **30**, 1971–1990 (2016).
36. Heizmann, B., Kastner, P. & Chan, S. Ikaros is absolutely required for pre-B cell differentiation by attenuating IL-7 signals. *J. Exp. Med* **210**, 2823–2832 (2013).
37. Bernardi, C. et al. CD4(+) T cells require Ikaros to inhibit their differentiation toward a pathogenic cell fate. *Proc. Natl. Acad. Sci. USA* **118**, 10.1073/pnas.2023172118 (2021).
38. Lee, J. Y. et al. Reprogramming anchorage dependency to develop cell lines for recombinant protein expression. *Biotechnol. J.* **19**, e2400104 (2024).
39. Kucia, M. et al. Bone marrow as a home of heterogenous populations of nonhematopoietic stem cells. *Leukemia* **19**, 1118–1127 (2005).
40. Huang, S. et al. An improved protocol for isolation and culture of mesenchymal stem cells from mouse bone marrow. *J. Orthop. Transl.* **3**, 26–33 (2015).
41. Leibovich, S. J. et al. Macrophage-induced angiogenesis is mediated by tumour necrosis factor-alpha. *Nature* **329**, 630–632 (1987).
42. Pujol, F. ernandez et al. K. Dendritic cells derived from peripheral monocytes express endothelial markers and in the presence of angiogenic growth factors differentiate into endothelial-like cells. *Eur. J. Cell Biol.* **80**, 99–110 (2001).
43. Schmeisser, A. et al. Monocytes coexpress endothelial and macrophagocytic lineage markers and form cord-like structures in Matrigel under angiogenic conditions. *Cardiovasc Res* **49**, 671–680 (2001).
44. Kelley, C. M. et al. Helios, a novel dimerization partner of Ikaros expressed in the earliest hematopoietic progenitors. *Curr. Biol.* **8**, 508–515 (1998).
45. Niu, J., Wang, K., Zhelyabovska, O., Saad, Y. & Kolattukudy, P. E. MCP-1-induced protein promotes endothelial-like and angiogenic properties in human bone marrow monocytic cells. *J. Pharm. Exp. Ther.* **347**, 288–297 (2013).
46. Brazelton, T. R., Rossi, F. M., Keshet, G. I. & Blau, H. M. From marrow to brain: expression of neuronal phenotypes in adult mice. *Science* **290**, 1775–1779 (2000).
47. Vierhout, M. et al. Monocyte and macrophage derived myofibroblasts: Is it fate? A review of the current evidence. *Wound Repair Regen.* **29**, 548–562 (2021).
48. Roybon, L. et al. Failure of transdifferentiation of adult hematopoietic stem cells into neurons. *Stem Cells* **24**, 1594–1604 (2006).
49. Canu, G. & Ruhrberg, C. First blood: the endothelial origins of hematopoietic progenitors. *Angiogenesis* **24**, 199–211 (2021).
50. Fadlullah, M. Z. H. et al. Murine AGM single-cell profiling identifies a continuum of hemogenic endothelium differentiation marked by ACE. *Blood* **139**, 343–356 (2022).
51. Neo, W. H. et al. Single-cell profiling reveals three endothelial-to-hematopoietic transitions with divergent isoform expression landscapes. *Nat. Cardiovasc Res* **4**, 1642–1661 (2025).
52. Lu, G. et al. The myeloma drug lenalidomide promotes the cereblon-dependent destruction of Ikaros proteins. *Science* **343**, 305–309 (2014).
53. Kronke, J. et al. Lenalidomide causes selective degradation of IKZF1 and IKZF3 in multiple myeloma cells. *Science* **343**, 301–305 (2014).
54. Wang, E. S. et al. Acute pharmacological degradation of Helios destabilizes regulatory T cells. *Nat. Chem. Biol.* **17**, 711–717 (2021).
55. Cai, Q., Dierich, A., Oulad-Abdelghani, M., Chan, S. & Kastner, P. Helios deficiency has minimal impact on T cell development and function. *J. Immunol.* **183**, 2303–2311 (2009).
56. Badea, T. C. et al. New mouse lines for the analysis of neuronal morphology using CreER(T)/loxP-directed sparse labeling. *PLoS One* **4**, e7859 (2009).
57. Dupe, V. et al. In vivo functional analysis of the Hoxa-1 3′ retinoic acid response element (3′RARE). *Development* **124**, 399–410 (1997).
58. Mastio, J. et al. Ikaros cooperates with Notch activation and antagonizes TGFbeta signaling to promote pDC development. *PLoS Genet* **14**, e1007485 (2018).
59. Dobin, A. et al. STAR: ultrafast universal RNA-seq aligner. *Bioinformatics* **29**, 15–21 (2013).
60. Satija, R., Farrell, J. A., Gennert, D., Schier, A. F. & Regev, A. Spatial reconstruction of single-cell gene expression data. *Nat. Biotechnol.* **33**, 495–502 (2015).
61. Klimmeck, D. et al. Transcriptome-wide profiling and post-transcriptional analysis of hematopoietic stem/progenitor cell differentiation toward myeloid commitment. *Stem Cell Rep.* **3**, 858–875 (2014).
62. Zhou, Y. et al. Metascape provides a biologist-oriented resource for the analysis of systems-level datasets. *Nat. Commun.* **10**, 1523 (2019).
63. Kirstetter, P., Thomas, M., Dierich, A., Kastner, P. & Chan, S. Ikaros is critical for B cell differentiation and function. *Eur. J. Immunol.* **32**, 720–730 (2002).
64. Zhang, Y. et al. Model-based analysis of ChIP-Seq (MACS). *Genome Biol.* **9**, R137 (2008).
65. Li, Q. H., Brown, J. B., Huang, H. Y. & Bickel, P. J. Measuring reproducibility of high-throughput experiments. *Ann. Appl. Stat.* **5**, 1752–1779 (2011).
66. Yu, G. C., Wang, L. G. & He, Q. Y. ChIPseeker: an R/Bioconductor package for ChIP peak annotation, comparison and visualization. *Bioinformatics* **31**, 2382–2383 (2015).
67. Ross-Innes, C. S. et al. Differential oestrogen receptor binding is associated with clinical outcome in breast cancer. *Nature* **481**, 389–U177 (2012).
68. Hortelano, S. et al. ILK mediates LPS-induced vascular adhesion receptor expression and subsequent leucocyte trans-endothelial migration. *Cardiovasc Res* **86**, 283–292 (2010).

Acknowledgements

We are grateful to D. Riveline for valuable advice. We thank members of the Chan-Kastner lab for scientific discussions and help, P. Marchal for technical support, the GenomEast platform for sequencing, C. Keime for help with the RNA-seq data analysis, S. Le Gras for help with ChIp-seq analyses, the CytoEast flow cytometry platform (C. Ebel, M. Philipps), the Institut Clinique de la Souris (M.C. Birling) for mouse generation, the IGBMC animal facility (M. Gendron, S. Falcone, W. Magnant, A. Vincent), and the PluriCellEast cell culture facility. HPC7 cells were kindly provided by L. Carlsson (University of Umeå, Sweden).

Author contributions

C.T., G.B., M.E.K., and P. Kirstetter performed the experiments. C.T., G.B., M.E.K., M.C.R.-M., P. Kirstetter, P.Ka. and S.C. analyzed the data. N.C.-W., P. Ki., P. Ka., and S.C. supervised the work. C.T., G.B., P. Kirstetter, P. Kastner, and S.C. designed the study. P. Ki., P. Ka., and S.C. wrote, and all authors reviewed the manuscript.

Funding

The authors received funding from the Agence Nationale de la Recherche (ANR-17-CE15-0023-01, ANR-22-CE15-0017 to S.C. and P. Kastner), the Fondation pour la Recherche Médicale (Equipe FRM 2019, EQU201903007812 to S.C. and P. Kastner), the EU Horizon 2020 research and innovation program under the Marie Sklodowska-Curie Initial Training Network ARCH (EU-H2020-MSCA-ITN-2018-813091 to P. Kastner and N.C.-W.), the EU-H2020-MSCA-COFUND EURIdoc programme (No. 101034170 to S.C.), La Ligue Contre le Cancer (LNCC)-

Comité Départemental 67 (MD/SP N°01 R.2023 to P. Kirstetter), an equipment grant from LNCC Grand Est/Bourgogne Franche Comté, institute funds from INSERM, CNRS, Université de Strasbourg (Unistra). This work received support from the Interdisciplinary Thematic Institute (ITI) IMCBio program from the University of Strasbourg, CNRS, and INSERM, which is supported by IdEx Unistra [(ANR-10-IDEX-0002), SFRI-STRAT'US (ANR-20-SFRI-0012) and EUR IMCBio (ANR-17-EURE-0023)]. C.T. was supported by predoctoral fellowships from EU-H2020-MSCA-ITN ARCH, ANR-10-LABX-0030-INRT grant, and Fondation ARC. M.C.R.-M. was supported by a predoctoral fellowship from EU-H2020-MSCA-ITN ARCH. G.B. was supported by a predoctoral fellowship from the French Ministère de l'Enseignement Supérieur et de la Recherche (MESR), M.E.K. was supported by a predoctoral fellowship from the EU-H2020-MSCA-COFUND EURIdoc programme, Unistra, and ANR-22-CE15-0017.

Competing interests
The authors declare no competing interests.

Additional information
Supplementary information The online version contains supplementary material available at https://doi.org/10.1038/s41467-026-78726-z.

Correspondence and requests for materials should be addressed to Susan Chan, Philippe Kastner or Peggy Kirstetter.

Peer review information *Nature Communications* thanks the anonymous reviewer(s) for their contribution to the peer review of this work. A peer review file is available.

Reprints and permissions information is available at http://www.nature.com/reprints

Publisher's note Springer Nature remains neutral with regard to jurisdictional claims in published maps and institutional affiliations.

Open Access This article is licensed under a Creative Commons Attribution 4.0 International License, which permits use, sharing, adaptation, distribution and reproduction in any medium or format, as long as you give appropriate credit to the original author(s) and the source, provide a link to the Creative Commons licence, and indicate if changes were made. The images or other third party material in this article are included in the article's Creative Commons licence, unless indicated otherwise in a credit line to the material. If material is not included in the article's Creative Commons licence and your intended use is not permitted by statutory regulation or exceeds the permitted use, you will need to obtain permission directly from the copyright holder. To view a copy of this licence, visit http://creativecommons.org/licenses/by/4.0/.

© The Author(s) 2026

This Article in Press is shared early to give you faster access to new research. It is citable and carries a permanent DOI. The final edited version will replace it automatically.